Spintronic Memristor as Interface Between DNA and Solid State Devices

Jianlei Yang, *Student Member, IEEE*, Zhenyu Sun, *Student Member, IEEE*, Xiaobin Wang, *Member, IEEE*, Yiran Chen, *Member, IEEE*, and Hai Li, *Member, IEEE*

***Abstract*—Recently biomolecular computing platforms have been widely investigated with great potentials in both biomedical research and practices, such as using molecular structures of DNA to present the data bits and to operate the logic. Emerging CMOS/molecular hybrid (CMOL) circuitry demonstrates many overwhelming advantages compared with pure biomolecular circuitry, including the design flexibility and compatibility with the traditional CMOS process. In this work, spintronic devices are utilized to detect the spatial information of DNA by translating the magnetic signals associated with the DNA pieces to electrical signals. The physical mechanisms and sensing performances of various magnetic sensor structures are discussed and evaluated, including giant magneto-resistance (GMR) spin valve sensors, tunnel magneto-resistance (TMR) sensors and our newly proposed spintronic GMR/TMR memristor sensors. A on-chip readout scheme is also proposed with a telecommunication method-frequency division multiplexing (FDM) technique to efficiently transmit useful information and filtrate the noise which could achieve high SNR up to 70 dB. The new approach can be adopted as not only the interface between the DNA structure and CMOS circuitry, but also a promising sensing mechanism in the DNA hybridization detection technique.**

***Index Terms*—DNA detection, memristor, spintronic.**

I. Introduction

MAGNETIC sensing is widely used in various modern bio-medical devices since many physiological behaviors/functions (e.g., nerve impulses) generate electrical currents along with magnetic field [1]. Monitoring such signals by detecting the magnetic fields is less invasive and more reliable than implanting electrodes to sense electronic signals. Generally, magnetic sensors can be utilized to detect the changes or disturbances of magnetic filed, i.e., the strength or direction of magnetic flux. For example, magnetic sensors with high sensitivity have been widely used in heart disease monitor by detecting the bio-magnetic signals from the heart (known as magnetocardiography, or MCG) [2], [3]. The magnetic sensors in bio-medical applications are required to detect the low-field signals that are much weaker than the earth's magnetic field ($<$ 0.5 Oe) [4].

Compared with other low-field sensing techniques, such as search coil, flux gate, and super-conducting quantum interference detectors (SQUID) [5]–[7], solid state sensors have demonstrated many unique advantages, including smaller size ($<$ 0.1 mm^2), lower power consumption, higher sensitivity ($\sim$ 0.1 Oe) and good compatibility with CMOS technology [4]. A solid state magnetic sensor can directly convert magnetic field into its resistance variation, which can be easily detected by applying a sense current or voltage.

The giant magnetoresistance (GMR) spin valve sensor and tunnel magnetoresistance (TMR) sensor are two major solid state magnetic sensor technologies widely used for low magnetic field detection. In both techniques, the relative angle of the magnetization directions of two ferromagnetic layers changes in the presence of magnetic fields, leading to the resistance variation of the sensor. The GMR and TMR technologies have been successfully utilized in the recording head of hard disk drive (HDD) for almost two decades [8]. Since the techniques of integrating GMR/TMR sensors with CMOS VLSI circuitry have been well developed, fabricating a large TMR/GMR micro-array becomes economically feasible to realize some complicated sensing systems. For example, a GMR sensor array was designed for DNA assay [9], [10]. The DNA samples being detected are pre-labeled/tagged by magnetic nanoparticles. DNA labeling is a kind of techniques for tracking biomolecules. After labeled, we could use electro-magnetic sensors to detect the changes and measure current between the targets. For more details of biomolecules sensing please refer to [11], [12]. Under an external magnetic field, the GMR sensor array can capture the magnetic response of the nanoparticles, which reflect the density and distributions of DNA samples.

However, magnetic particle labels with micron or sub-micron size are not able to meet the requirement of ultra high bio-detection sensitivity such as single molecule detection [13]. Especially for DNA fragments detection, the dimension of magnetic particle labels should be 20 nm or smaller in diameter [14]. Because the dimension of nanoparticles/nanotags are comparable to that of the target DNA molecules, the utilization of nanoparticles with a diameter of $100 \sim 1000$ $\mathring{A}$ is attracting for magneto-nano biochip. In addition, the nanoparticles are excited by modulating magnetic field which can reduces the impact of $1/f$ noise, enabling useful signal detection in a limited frequency band. On the other hand, detecting such tiny magnetic nanotags

Manuscript received on June 01, 2015; revised August 20, 2015, and October 19, 2015; accepted November 15, 2015, and November 18, 2015. Date of publication April 20, 2016; date of current version June 09, 2016. This work was supported in part by DARPA D13AP00042, NSF 1311706, and NSF 1337198. This paper was recommended by Guest Editor S. Ghosh.

J. Yang, Y. Chen, and H. Li are with the Department of Electrical and Computer Engineering, University of Pittsburgh, Pittsburgh, PA 15260 USA (e-mail: jiy64@pitt.edu; yic52@pitt.edu; hal66@pitt.edu).

Z. Sun is with the Broadcom Corporation, Irvine, CA 92617 USA (e-mail: sunzhenyu223@gmail.com).

X. Wang is with the Avalanche Technology, Fremont, CA 94538 USA (e-mail: martinying@gmail.com).

Color versions of one or more of the figures in this paper are available online at http://ieeexplore.ieee.org.

Digital Object Identifier 10.1109/JETCAS.2016.2547700

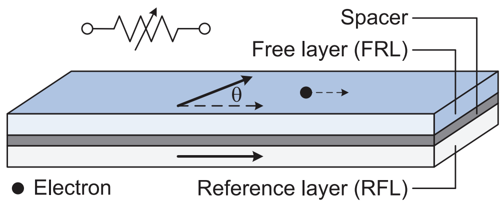

Fig. 1. GMR spin valve sensor structure.

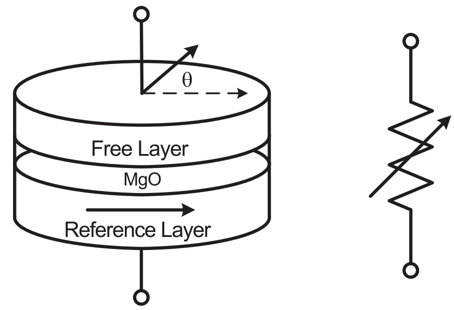

Fig. 2. MTJ device structure.

with limited physical volume is a challenge to the detectors, because their magnetic moments are very small and constrained by external impact such as noise and thermal turbulence. Hence, a high performance detector with ultra high sensitivity and resolution is required for mass-produced magnetic micro-array.

Besides TMR and GMR devices-based sensor, another emerging nonvolatile device — memristor is also very promising in the nanoparticle detection. Especially, the recent proposal domain wall motion-based spintronic memristor [15] can change its memristance/resistance when responding to its external electrical or magnetic excitation. Unlike GMR and TMR sensors, the resistance states of memristor still maintain even the external excitations are removed. Due to the different magnetic and electrical characteristics among TMR, GMR, and spintronic memristor, operating mechanisms of these devices are also different. A spintronic memristor-based sensing mechanism was proposed in [16] which has different relative resistance change, noise, sensitivity, reliability compared to TMR and GMR sensors. Compared with [16], corresponding optimization philosophy is discussed and evaluated in this work: 1) More details of the FDM approach and implementations are demonstrated, which is important for the readers to understand how the noise endurability of the design is measured; 2) Two kinds of noise sources are evaluated and additional simulations are conducted to optimize the sensing SNR with proper time slots, which provides some comprehensive technical references for practical design.

The rest of this paper is organized as follows. Section II provides the fundamentals of GMR/TMR sensor and spintronic memristor, as well as the application of magnetic sensors in DNA assay. Section III describes the proposed magnetic sensing mechanism of spintronic memristors. Section IV discuss the design tradeoffs of different devices by using DNA assay as the example. Section V demonstrates the proposed readout scheme and the noise endurability. Concluding remarks are given in Section VI.

II. Preliminary

A. GMR and TMR Sensors

A typical GMR spin valve sensor is shown in Fig. 1. A long spin-valve strip includes two ferromagnetic layers—reference layer (RFL) and free layer (FRL), which are separated by a thin non-ferromagnetic spacer, e.g., AlO. The magnetization direction (MGD) of RFL is fixed by coupling to a pinned magnetic layer while the MGD of FRL changes in the presence of magnetic field. The resistance of a GMR sensor is determined by the relative angles between the MGD of RFL and FRL. If the MGD between RFL and FRL is parallel/anti-parallel to each other, the total resistance of the GMR sensor reaches its minimum/maximum value. In a GMR spin valve structure, the electrons travel with their spins orientated parallel to the ferromagnetic layers. For a typical TMR device, such as — magnetic tunneling junction (MTJ) as shown in Fig. 2, two ferromagnetic layers are separated by an oxide barrier layers, e.g., MgO. Different from GMR devices, the electrons travel with their spins orientated perpendicularly to the layers across the oxide barrier. Under the applied external magnetic field or injected spin current, the MGD of FRL is biased from the stable orientations (parallel or antiparallel to the MGD of RFL) and leads to the device resistance changes.

Usually we define the magnetoresistance ratio of TMR/GMR devices as $MR = (R_H - R_L)/R_L$. Here R_H and R_L represent the resistances of the magnetic device when the MGDs of two ferromagnetic layers are anti-parallel and parallel, respectively. The resistances of TMR/GMR devices vary between R_L and R_H in the presence of magnetic field. The exact resistance value that is determined by the direction and amplitude of the magnetic field can be detected by applying a small sensing current through the device and measuring the voltage across it. Consequently a larger MR may be helpful for better sensing performance. After the sensed magnetic field is removed, TMR/GMR devices will return back to its stable states, at which the MGD of FRL is parallel or anti-parallel to that of RFL.

B. Spintronic Memristor

As early as year 1971, Prof. L. Chua predicted the existence of memristor based on the completeness of circuit theory. Besides resistor, capacitor and inductor, there must be a fourth fundamental passive circuit element to bridge the electrical charge (q) and the magnetic flux (ϕ) [17]. The element was named as memristor. The corresponding physical variable—memristance (M) is uniquely determined by the historic profile of the applied voltage on the device or injected current through it.

The memristor can be realized by many different materials, such as Mn-doped ZnO films [19], Pt/$BiFeO_3$/Nb-doped $SrTiO_3$ [20], or even carbon nanotube [21]. The spintronic memristor proposed in [18] is shown in Fig. 3. The whole structure is similar as the GMR sensor except that the free layer is divided by a magnetic domain-wall into two segments that have opposite magnetization directions to each other. When applying a current to the spintronic memristor, the domain wall can move in the longitudinal direction. Because of the different resistance per unit length at the two sides of domain wall, the

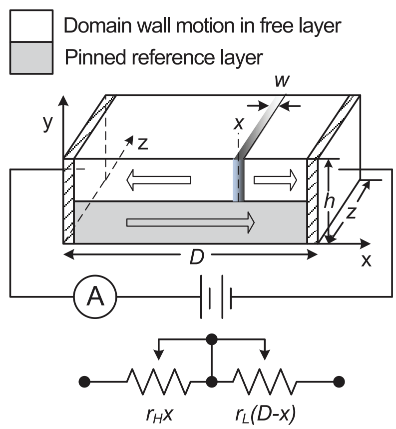

Fig. 3. Spintronic memristor based on magnetic domain-wall motion [18].

total device resistance/memristance varies from R_L to R_H, when the domain wall moves from $X(t) = 0$ to $X(t) = D$. Here D is the device length. $X(t)$ is the domain wall position at time t. In general, the device resistance can be calculated as

$$R(t) = R_H - \frac{(R_H - R_L)\, X(t)}{D}. \tag{1}$$

We note that the domain-wall movement happens only when the applied current density J is larger than critical current density J_{cr}. Also, the domain wall velocity v is proportional to the current density J. Besides the spin torque excitation generated by electrical current, the domain wall mobility is also affected by the thermal fluctuation and the applied magnetic field [18]. Under certain conditions, the amplitude of magnetic field can be sensed as the resistance of the spintronic memristor (or the domain wall location). As an obvious advantage of spintronic memristor, the device state, i.e., the domain wall location, will maintain after the sensed magnetic field is removed.

C. Magnetic Sensor Micro-Array for DNA Assay

The principle of magnetic sensor micro-array based DNA assay [22] is shown in Fig. 4. Single-stranded DNA receptors (or known as DNA probes) are immobilized on the surface of a magnetic sensor micro-array. The unknown DNA fragments (targets) are labeled by high moment magnetic nano-particles (nano-tags) with some binding technique, e.g., biotin-streptavidin chemistry. During DNA detection, the tagged DNA fragments (targets) are captured by the complimentary DNA probes. To detect the density and the distribution of the DNA targets, nano-particles are excited by applying an external magnetic field and their corresponding magnetic responses are sensed by the magnetic sensor array.

III. Spintronic Memristor Based Magnetic Sensing

The spin torque induced domain wall motion at finite temperature can be described by stochastic Landau–Lifshitz–Gilbert (LLG) equation [23] with a spin torque term [24]. Using rigid wall approximation [25], the domain wall motion is expressed in terms of magnetization spherical angle θ and ϕ as

$$\theta(x,t) = \theta_0\left(x - X(t)\right), \tag{2}$$

$$\phi(x,t) = \phi_0(t) \tag{3}$$

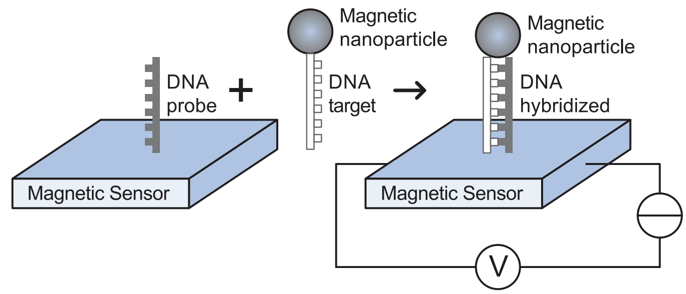

Fig. 4. Magnetic sensor micro-array for DNA assay.

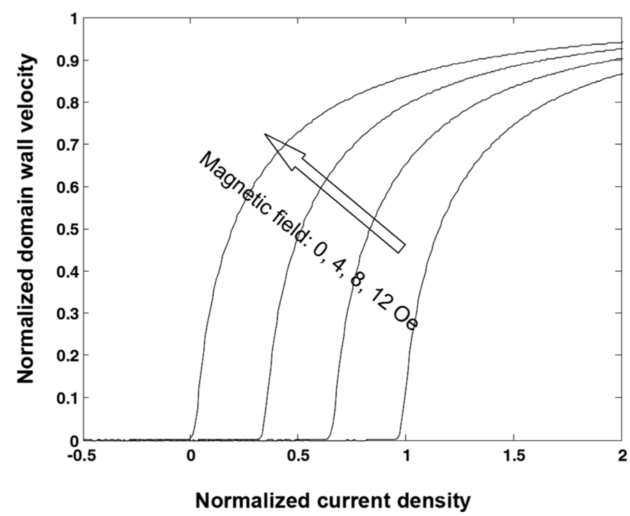

Fig. 5. Normalized domain wall velocity as a function of the normalized current density under the different magnetic fields at 300 K.

where $\theta_0(x) = \arccos[\tan(x/w)]$ is the function of domain wall shape. w is the domain wall thickness. $X(t)$ is the domain wall position. Domain wall velocity $v = dX(t)/dt$. The domain wall position $X(t)$ satisfies following stochastic differential equations [25]:

$$\frac{d\phi}{dt} + \frac{\alpha}{w}\frac{dX}{dt} = \gamma H + \eta_\phi, \tag{4}$$

$$\frac{1}{w}\frac{dX}{dt} - \alpha\frac{d\phi}{dt} = w_0 \sin(2\phi) + \frac{V_s}{w} + \eta_x \tag{5}$$

where $w_0 = \gamma H_p/2$, γ is gyro-magnetic ratio, α is the damping parameter, H is the magnetic field including external unbalanced field and intrinsic domain wall pinning field. $v_s = PJ\mu_B/eM_s$ is the spin torque excitation strength, P is the polarization efficiency, μ_B is the Bohr magneton, and e is the elementary electron charge. η_ϕ and η_x are the ϕ and X components of the thermal fluctuation fields, respectively. Spintronic memristors sense the magnetic field change between the labeled nano-particles (with magnetic injected) and the unlabeled nano-particles (without magnetic injected) [26]. Fig. 5 demonstrates the normalized domain wall velocity as a function of the normalized current density under different magnetic fields at 300 K. The magnetic field is the additional field due to the existence of the bound magnetic nano-particles. When the applied current density is close to the critical one J_{cr}, the domain wall velocity becomes very sensitive to the amplitude of the applied external magnetic field. During the

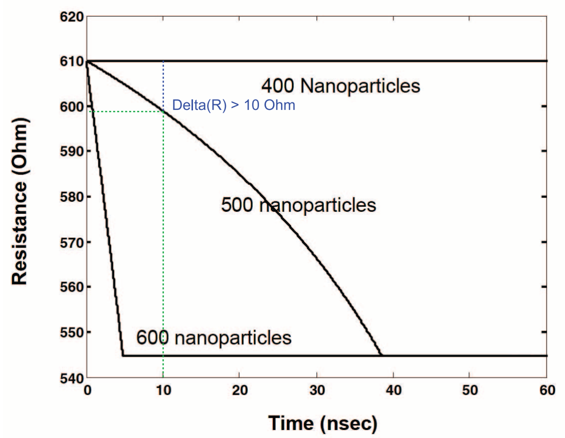

Fig. 6. Spintronic memristor resistance as a function of time under different number of magnetic nano-particles at 300 K.

sensing operation, a current with the density slightly below the critical current density J_{cr} is applied to spintronic memristor for certain duration.

The domain wall will move to the different locations under the different magnetic fields excited by the bound magnetic nano-particles. Fig. 6 shows the spintronic memristor resistance as a function of time under the different number of magnetic nano-particles at 300 K. Based upon [26], the amplitude of magnetic field generated by nano-particles is approximately proportional to nano-particle numbers. 500 nano-particles in Fig. 6 corresponds to a magnetic field around 10 Oe at the spintronic domain wall center.

IV. Design Space Exploration

A. Biosensor Array Architecture

A popular biosensor array architecture can be similarly utilized for GMR, TMR and spintronic memristor as shown in Fig. 7. In our design, a DNA spot consists of $N \times N$ biosensor cells. The whole on-chip biosensor is composed of 4×4 DNA spots with the corresponding control bus. To increase the throughput of the biosensor array, both frequency division multiplexing (FDM) [27] and time division multiplexing (TDM) [28] are utilized [9]. In this architecture, every four DNA spots share one physical link with four carrier frequencies to realize FDM. Then all of the four FDM channels are connected to one 4-to-1 multiplexer to achieve TDM. The final output is sent to off-chip signal processing system to carry out Fourier transformation and frequency spectrum analysis.

B. Circuit Design

The circuit schematic of readout channel for biosensor is demonstrated in Fig. 8. The readout channel includes a read current source, a frequency divider, a mixer, a low noise differential amplifier, a programmable operational amplifier and a transmission gate-based multiplexer. The readout circuit is designed with PTM 90 nm technology node [26]. All circuit level simulations are conducted under Cadence Spectre Analog environment. The device models of GMR, TMR and spintronic memristor were developed by using Verilog-A language. For more details of GMR device model, the readers could refer to [29]. For TMR device model implementation, please refer to [30]. The spintronic memristor model and validation could found in [31].

During the readout operation, current source injects a small (i.e., 0.1 mA) read current into both the sensor cell (Act) and the reference resistance (Ref) to incur Act and Ref voltages, respectively. These two voltages are connected to the inputs of the mixer, which multiplies the readout voltage by sampling pulse (carrier frequency) generated by the frequency divider with a master clock of 20 kHz. As shown in Fig. 8, each DNA spot within one readout channel has its own carrier frequency. The low noise differential amplifier (DA) is used to amplify the voltage difference between the Act and Ref voltages. Furthermore, it can also serve as an analog adder by swapping the Act and Ref voltages at the inputs of the mixer. Thus, at the end of the each readout channel, the sensing signals (difference between Act and Ref voltages) of all the four DNA spots have been summed up to share one physical channel. In our design, FDM is realized by modulating the signals with different carrier frequencies, which can be extracted by off chip band pass filter. FDM can also reduce $1/f$ noise effectively. A programmable operational amplifier (POA) with a gain range from 10 to 60 is designed to maximize the dynamic range of the output signal. Instead of pushing the amplifier gain even higher, we use multi-level amplifiers to reduce design complexity and improve circuit reliability.

The simulated output signal of one read out channel is plotted in Fig. 9. The main clock frequency is set as 20 kHz. The four carrier frequencies are 20/6 kHz, 20/8 kHz, 20/10 kHz, and 20/12 kHz. To guarantee cycle integrality of all signals, the minimal time slot should cover integral multiples of all the carrier clock period, e.g., 6 ms in our configuration. The outputs of the four read out channels are connected to a 4-to-1 multiplexer. Each channel is assigned to a time slot to achieve TDM function. The baseline design parameters are summarized in Table I.

C. Comparison Among Different Devices

GMR, TMR, and spintronic memristor are all spintronic sensors. However, these devices demonstrate the different responses to extraneous magnetic field disturbances of nanoparticles in terms of the resistance value changing (ΔR) and the resistance transition time. Accordingly, the circuit design should be adjusted for each specific device as shown in Table II. The MR ratio of a typical GMR device is around 10% [32]. The minimum resistance gap before and after absorbing nano-particles could be only 100 mΩ, which results in only $\sim$ 10 μV voltage difference at the output of DNA spot. Thereby, the overall voltage gain of the amplifiers need be relatively high. Usually, a TMR device has a MR ratio of $\sim$ 100% or higher [8]. Hence, the resistance gap and voltage difference could be significantly improved.

For MTJ used in MRAM, the state of free layer could be maintained after removing the injection read/write current or external magnetic field because its spin direction has reached one of the two steady states (parallel or anti-parallel). But for GRM or TMR adopted in sensor applications, there is no two steady states assigned for them. Additionally, spintronic memristor can

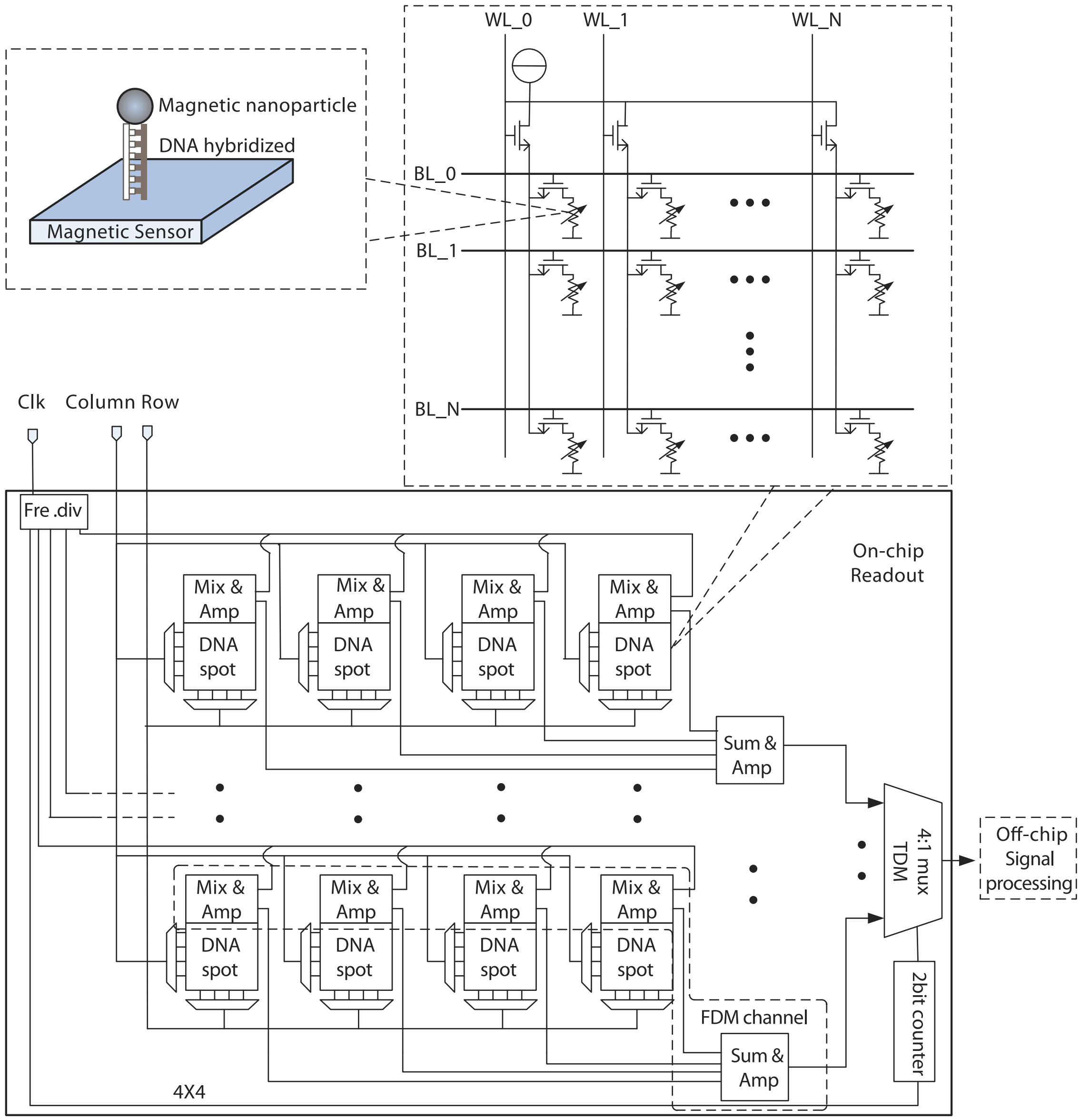

Fig. 7. Biosensor architecture design.

maintain the resistance states after removing the external magnetic fields. Note that the resistance gap (ΔR) of a memristor sensor can be adjusted by controlling the time period of apply external magnetic field as shown in Fig. 6. We assume the magnetic field applied for 10 ns with 500 magnetic nano-particles, and then the resistance gap ΔR could be more than 10 Ω as shown in Fig. 6.

As shown in Table II, the gain of differential amplifier and programmable operational amplifier can be adjusted accordingly. In GMR, due to the small ΔR (from 100 mΩ to 400 mΩ), we select the maximum gain for both DA with 3 and PGA with 60. Therefore the output voltage can be speculated by $\Delta R \times G_{DA}^3 \times G_{PGA}$, where G_{DA} is DA gain and G_{PGA} is PGA gain. If DA gain and PGA gain is 3 and 60 respectively, the output voltage could be range from 16.2 to 64.8 mV. Nevertheless, if all circuit parameters keep same but substituting GMR by TMR device, the maximum voltage will be 648 mV which is 10 times of GMR sensor. Under above situation, voltage signals of four DNA spots are summed up in FDM so that the total output could surpass VDD (1 V). Hence, the PGA gain and DA gain should be adjusted to a lower value. On the other hand, we have another constraint that the sum up of output voltages of four DNA spots cannot beyond the voltage swing (300 mV) of PGA otherwise the amplifier does not work at linear region. Moreover, the DA gain may need to be redesigned when different device is used (i.e., TMR, memristor). Decreasing in DA gain can not only address voltage swing issue but also save chip area. For example, the MOS transistor width of a DA with gain of 2 is 5 times smaller than that of a DA with gain of 3.

V. FDM Signal Processing and Noise Analysis

A. Modulation Theory and Implementation

In the previous section, we has discussed about combination of FDM and TDM scheme by using pulse sampling to achieve high throughput and low noise. In this section, we will further

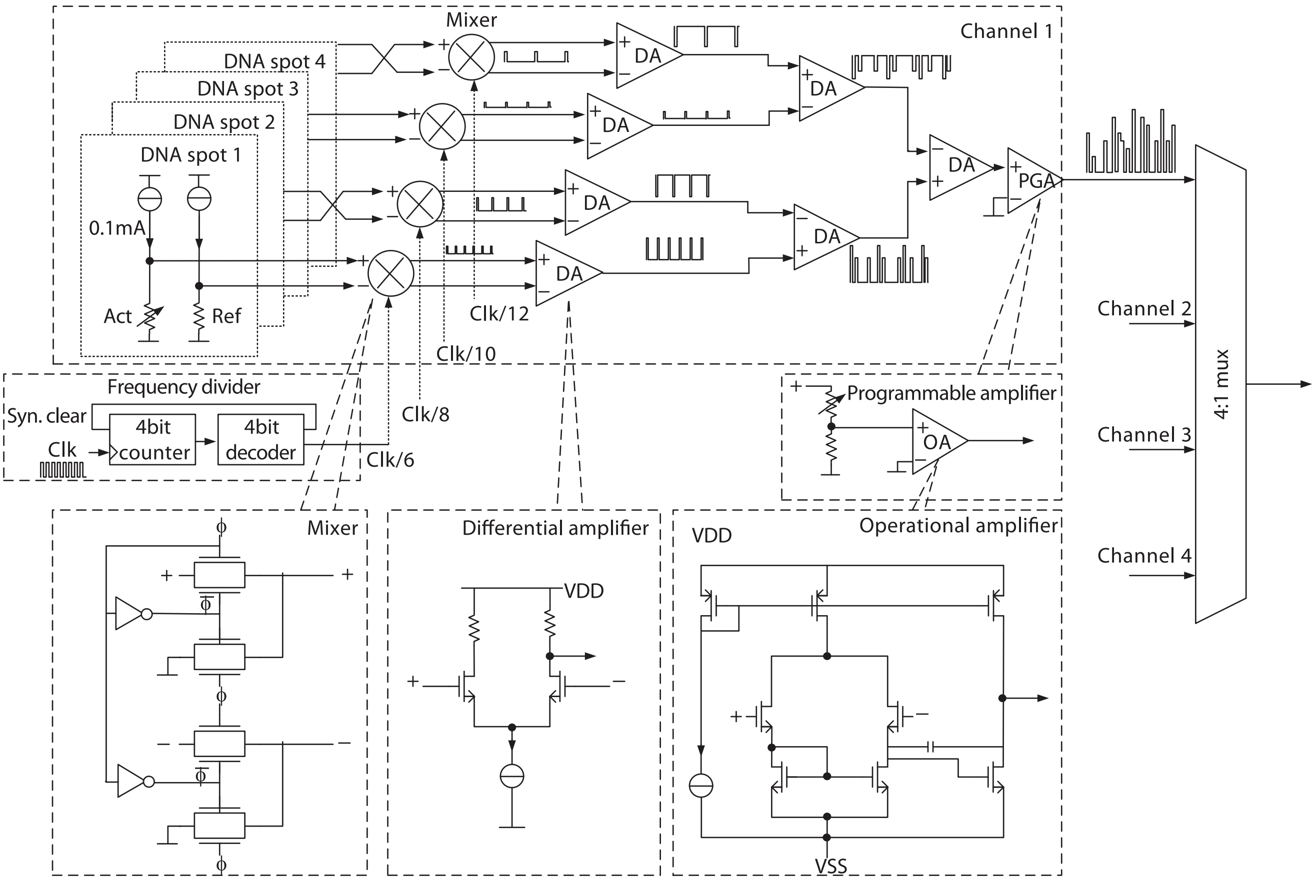

Fig. 8. Schematic of readout channel.

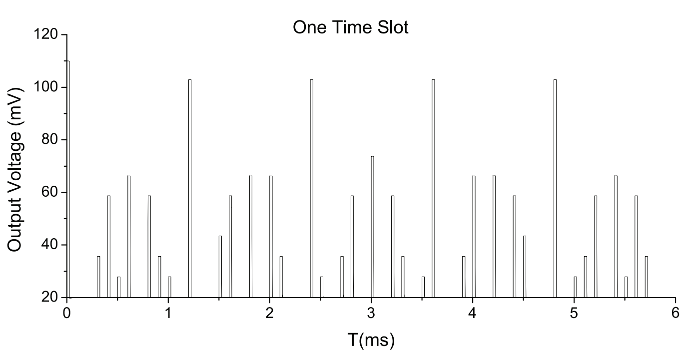

Fig. 9. Simulation result of 1 channel at output of PGA.

TABLE I
BASELINE CIRCUIT DESIGN PARAMETERS

Differential amp gain	2 or 3
Programmable operational amp gain	$10 \sim 60$
Output swing of operational amp (mV)	300
Main clk frequency and limitation (kHz)	20
Carrier frequencies for FDM (kHz)	3.33, 2.5, 2, 1.67
One time slot of TDM (ms)	6

TABLE II
CIRCUIT DESIGN PARAMETERS SPECIFIED TO THREE DEVICES

Device	ΔR $(m\Omega)$	DA gain	PGA gain	ΔV (mV)
GMR	$100 \sim 400$	$3 \times 3 \times 3$	60	$16.2 \sim 64.8$
TMR	$1000 \sim 5000$	$2 \times 2 \times 2$	10	$8 \sim 40$
Memristor	10000	$2 \times 2 \times 2$	10	80

improve the efficiency and leverage the noise endurability of the FDM modulation technology by using cosine signal which is originally developed for radio telecommunication. In its basic form, a signal with power concentrated at the carrier frequency will be produced. In modulation, message signal is multiplied by carrier signal which has a much higher frequency than the message signal, and is defined as

$$f\left(t\right)=m\left(t\right)\cdot\cos\left(2\pi\cdot f_0\cdot\frac{n}{f_s}\right). \tag{6}$$

where $m\left(t\right)$ is usually referred to as the message signal and f_0 is the carrier frequency. As shown in above equation, the modulation consists of multiplying the message signal $m\left(t\right)$ by the carrier $\cos\left(2\pi\cdot f_0\cdot n/f_s\right)$. Therefore, we can use the modulation theorem of Fourier Transforms to obtain the spectrum F (f) in frequency domain by calculate

$$F\left(f\right)=\frac{1}{2}\left[M\left(f-f_0\right)+M\left(f+f_0\right)\right] \tag{7}$$

where $F\left(f\right)$ is the Fourier Transform of $M(f)$. According to the property of Fourier Transform, multiplication of signals in time domain will result in their convolution in frequency domain. And the Fourier Transform of cosine function is shifted Dirac delta function, so the wave of message signal will be shifted to $-f_0$ and f_0. In the implementation of our biosensor circuit, the message signal is the voltage variation caused by the memristance changing of the micro-array spintronic memristor

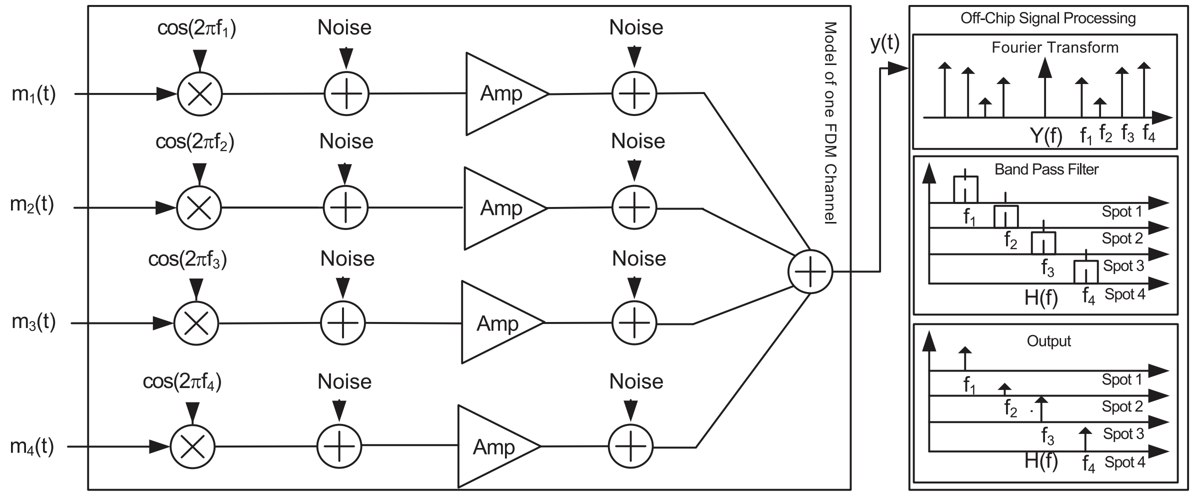

Fig. 10. FDM channel model.

detector. The voltage signal of each detection point will be multiplied by the a carrier frequency through the analog mixer. We have four DNA spots in one FDM channel, so totally four cosine signal with four different carrier frequencies are needed. They can be expressed by $f(t) = \sum_{i=1}^{4} m_i \cos(2 \cdot \pi \cdot f_i \cdot t)$. We still use the frequencies as shown in Table I. The benefit by using this FDM modulation technology is that most of the power of the signal will concentrate at the carrier frequency, therefore we can use bandpass filter to obtain the useful information and eliminate most of the noise at the same time.

We use simplified model to illustrate the FDM principle of circuit as shown in Fig. 10. Three-stage amplifiers in readout circuit of Fig. 8 are simplified into one ideal amplifier added with a noise source. And the mixer also brings in certain noise. The target signals $m_1(t)$ to $m_4(t)$ are four voltage levels (v_1 to v_4) generated by the memristor which is applied by a read current. As we have mentioned before, the output $y(t)$ will be TDM to off-chip signal processing, hinting that it is impossible for the time slot of each FDM channel to be infinite. With limited time period, the spectrum of the output signal in frequency domain can not be ideal Dirac delta function as shown in Fig. 10. In the following paper, we will show the simulation results with different lengths of time slots and different types of noise in order to measure the noise endurability of the design.

B. Noise Source

The detection performance variation is easily determined by two categories of factors: intrinsic variation and non-intrinsic variation. Intrinsic variation could be involved by the process variation when manufacturing the spintronic memristor, and non-intrinsic variation could be regarded as sensing noises. Process involved variation behaviors could be captured according to the manufacturing technology features [33], and additional constrains could be utilized to tolerate memristance variations [34]. Intrinsic variation is not taken into consideration in this work due to the lack of real devices models for reasonable process variation parameters of spintronic memristor. Since the intrinsic variation behaviors could be characterized and tolerate strategies are available for design optimization, we are more interested in exploring the non-intrinsic variation to evaluate the involved noises on bio-sensors. The noise behavior of the bio-chip is dominated primarily by two noise sources: thermal noise and pink or so-called $1/f$ noise. Thermal noise is approximately white, meaning that the power spectral density is nearly equal throughout the frequency spectrum. Additionally, the amplitude of the signal is similar with Gaussian probability density function. In the signal process simulation, we use white noise to approximately model the thermal noise. We can simulation stationary, continuous-time random process $x(t) : t$ is real with constant mean μ and covariance function

$$K_x(\tau) = E(x(t_1) - \mu)(x(t_2) - \mu)^* \tag{8}$$

where $\tau = t_1 - t_2$ and power spectral density

$$S_x(f) = \int_{-\infty}^{\infty} K_x(\tau) e^{-jw\tau} d\tau. \tag{9}$$

Pink noise or $1/f$ noise in current or voltage is always related to a direct current because it is a resistance fluctuation, which is transformed to voltage or current fluctuations via Ohm's law [35]. $1/f$ noise shows up a low-frequency phenomenon, as the high frequencies are overshadowed by white noise from other sources. The frequency spectrum of $1/f$ noise can be described as the power spectral density is inversely proportional to the frequency

$$N_f = \frac{\alpha}{N \cdot f} (I \cdot R)^2, \tag{10}$$

where α is the dimensionless (sometimes field dependent) Hooge constant, N is the total number of conduction electrons in the sensor (often taken as the number of atoms in the active area of the sensor), f is the frequency, I is the read current, and R is the resistance of micro sensor. [5] gave α values ranging from 6.7×10^{-3} to 2.8×10^{-1}.

We will show fast Fourier transform (FFT) of FDM voltage output mixed with above mentioned two noise. According to Nyquist sampling theory, sampling frequency must be at least

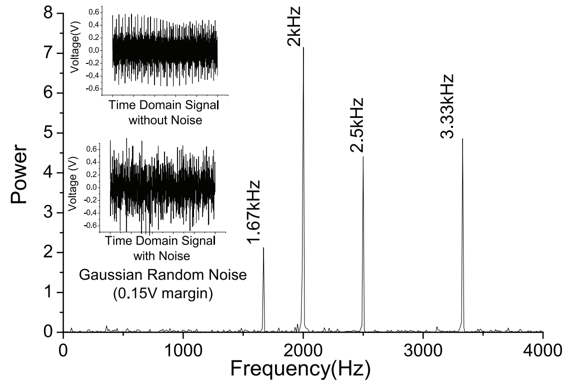

Fig. 11. Output power after Fourier Transform with Gaussian white noise.

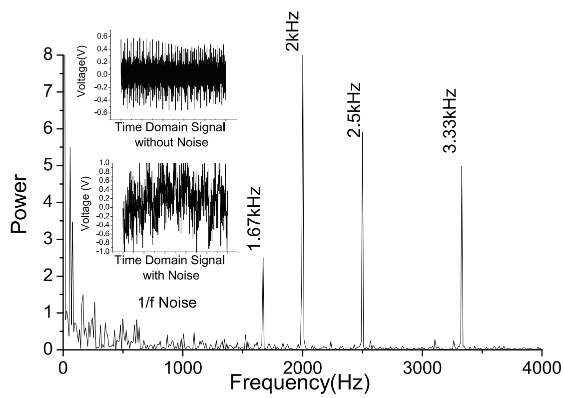

Fig. 12. Output power after Fourier transform with $1/f$ noise.

twice bigger than the message signal. The highest carrier frequency is 3.33 kHz, so we define the sampling frequency f_s to be 10 kHz in our simulation.

C. Simulation Results

Fig. 11 shows the FFT of FDM output with Gaussian random white noise. The main curve is in frequency domain. As we can see from the main curve, the four message signals are clearly centered at 1.67 kHz, 2 kHz, 2.5 kHz, and 3.33 kHz along with the frequency coordinate. Subgraphs shows the FDM output before FFT in time domain with and without white noise. As we can see, the impact of white noise in the time domain is very larger, while it is much more trivial in the frequency domain. Once we use bandpass filter to extract the useful information, the impact of the white noise will be even smaller. We will measure the signal-to-noise ratio (SNR) later to estimate the benefit brought by FDM in the bio-circuit readout. Fig. 12 shows the FFT of FDM output with $1/f$ noise. The power density of $1/f$ noise is gather around low frequency region and rolls off with the increasing of frequency. When the frequency beyond one kilo Hertz, the impact of $1/f$ noise turns to be very small. Subgraphs shows the FDM output before FFT in time domain with and without $1/f$ noise. Obviously, the impact of $1/f$ noise in time domain is much greater than that in the frequency domain that further prove the efficiency of FDM in eliminating noise influence.

In order to demonstrate the endurability of our scheme, signal-to-noise (SNR) is adopted as a measurement metric.

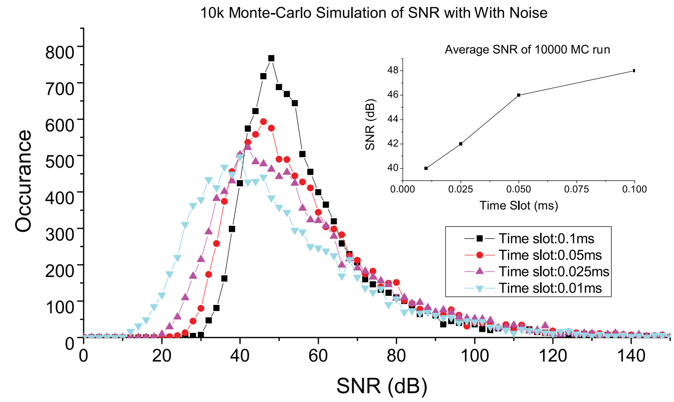

Fig. 13. Monte-Carlo simulation of SNR with Gaussian random noise.

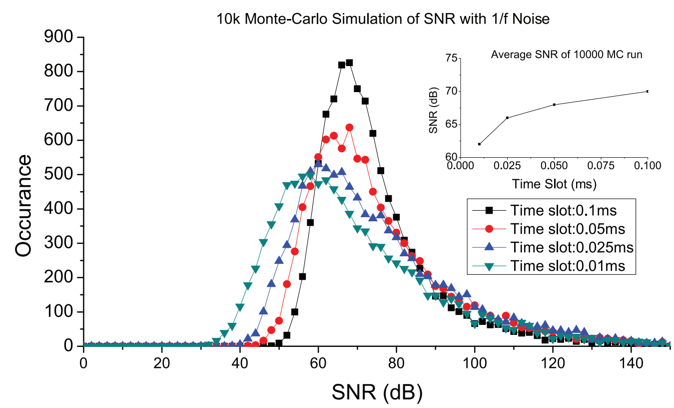

Fig. 14. Monte-Carlo simulation of SNR with $1/f$ noise.

Under the impact of Gaussian random white noise, the SNR can be calculated by

$$SNR_{white} = 10 \log \left(\frac{\sum_{i=1}^{4} \left(I \Delta R_i \times \cos\left(2\pi f_i t\right) \right)^2}{\int_{-\infty}^{\infty} K_x\left(\tau\right) e^{-jw\tau} d\tau} \right) \tag{11}$$

where I is the read current, ΔR_i is the resistance change of each detection device.

Fig. 13 shows the 10^4-run Monte-Carlo simulation of SNR with Gaussian random white noise. Four lengths of time slot are compared in the simulation. The larger the time slot is, the higher the SNR will be. That is because larger time slot implies the closer the Fourier transform will be to the Dirac delta function at frequency domain. Because we use ideal bandpass filters whose center frequencies are 1.67 kHz, 2 kHz, 2.5 kHz, and 3.33 kHz with bandwidth of 200 Hz. Therefore, the power of the output signal physically concentrates more at certain frequency point resulting in high SNR after passing the ideal bandpass filter. However, larger time slot means low throughput, so tradeoff between SNR and throughput has to be balanced according to requirement. Because the resistance changing of GMR and TMR device is relatively small, so the impact of noise will become bigger in return. When GMR and TMR are used as bio-sensor interface, we will give more priority to SNR. For spintronic memristor, the resistance changing is much larger than GMR or TMR device, so the SNR is reasonably high as we can see from the simulation. When the time slot is 0.1 ms, the SNR can approach almost 50 dB. That means the power of useful information is 316.22 times of the power of noise. If we want to improve the throughput, we can tune the time slot to be 0.01 ms. In other word, we can obtain information of four detection spots in every 10 microseconds, and the corresponding SNR also stays as high as 40 dB.

Under the impact of $1/f$ noise, the SNR can be calculated by

$$SNR_{1/f} = 10\log\left(\frac{\sum_{i=1}^{4}\left(I\Delta R_i \times \cos\left(2\pi f_i t\right)\right)^2}{\frac{\alpha}{(N_f\Delta f)I^2R^2}}\right) = 20\log\left(\frac{\sum_{i=1}^{4} I\Delta R_i \times \cos\left(2\pi f_i t\right)}{\sqrt{\frac{\alpha}{(N_f\Delta f)IR}}}\right). \quad (12)$$

Fig. 14 shows the 10^4-run Monte-Carlo simulation of SNR with $1/f$ noise. When the time slot is selected as 0.1 ms, the SNR can reach 70 dB. The reason behind is when frequency surpasses 1 kHz, the $1/f$ noise levels off to zero. We also compared SNR before bandpass filter and after bandpass filter. The bandpass filter can help improve SNR_{white} and $SNR_{1/f}$ by 3.4 and 5.83 times respectively when one time slot period is 0.01 ms. Obviously, the improvement of $SNR_{1/f}$ is larger than of SNR_{white} because the power of $1/f$ noise is gathered at low frequency region and most of them is filtered by the bandpass filter.

VI. Conclusion

In this work, we discuss a possible magnetic field sensing mechanism of spintronic memristors, which can be utilized in DNA hybridization detection. The circuit implementation of a biosensor array based on spintronic memristors is also proposed. We compare the differences between spintronic memristors and the other two popular spintronic devices—GMR and TMR, in terms of working mechanism, magnetic and electric parameters etc. Our analysis show that besides the nonvolatility (the sensed value is kept in the device after the sensed magnetic field is removed), spintronic memristors also show a higher sensing signal amplitude than TMR and GMR devices. We also propose a on-chip readout scheme with a telecommunication method-frequency division multiplexing (FDM) technique that can efficiently transmit useful information and filtrate the noise. We can achieve high SNR up to 70 dB by using proposed scheme.

Acknowledgment

Any opinions, findings and conclusions or recommendations expressed in this material are those of the authors and do not necessarily reflect the views of DARPA, NSF, or their contractors.

References

[1] A. Cooper, E. Magesan, H. Yum, and P. Cappellaro, "Time-resolved magnetic sensing with electronic spins in diamond," *Nature Commun.*, vol. 5, 2014.

[2] S. Lau, R. Eichardt, L. Di Rienzo, and J. Haueisen, "Tabu search optimization of magnetic sensor systems for magnetocardiography," *IEEE Trans. Magnet.*, vol. 44, no. 6, pp. 1442–1445, Jun. 2008.

[3] M. Pannetier-Lecoeur *et al.*, "Magnetocardiography with sensors based on giant magnetoresistance," *Appl. Phys. Lett.*, vol. 98, no. 15, p. 153705, 2011.

[4] C. H. Smith and R. Schneider, "Low magnetic field sensing with GMR sensors, Part 1: The theory of solid-state magnetic sensing," *Sensors Mag.*, 1999.

[5] A. Rhouni, G. Sou, P. Leroy, and C. Coillot, "Very low $1/f$ noise and radiation-hardened CMOS preamplifier for high-sensitivity search coil magnetometers," *IEEE Sensors J.*, vol. 13, no. 1, pp. 159–166, Jan. 2013.

[6] L. Rovati and S. Cattini, "Contactless two-axis inclination measurement system using planar flux-gate sensor," *IEEE Trans. Instrum. Meas.*, vol. 59, no. 5, pp. 1284–1293, May 2010.

[7] M. Takemoto, T. Akai, Y. Kitamura, Y. Hatsukade, and S. Tanaka, "HTS Rf-squid microscope for metallic contaminant detection," *IEEE Trans. Appl. Superconduct.*, vol. 21, no. 3, pp. 432–435, Jun. 2011.

[8] S. Mao *et al.*, "Commercial TMR heads for hard disk drives: Characterization and extendibility at 300 $\mathrm{Gbit/in^2}$," *IEEE Trans. Magn.*, vol. 42, no. 2, pp. 97–102, Feb. 2006.

[9] S. Han *et al.*, "CMOS integrated DNA microarray based on GMR sensors," in *Proc. Int. Electron Devices Meet.*, 2006, pp. 1–4.

[10] W. Wang *et al.*, "Surface modification for protein and DNA immobilization onto GMR biosensor," *IEEE Trans. Magn.*, vol. 49, no. 1, pp. 296–299, Jan. 2013.

[11] P. M. Levine, P. Gong, K. L. Shepard, and R. Levicky, "Active CMOS array for electrochemical sensing of biomolecules," in *Proc. CICC*, 2007, pp. 825–828.

[12] S. Petralia and G. Ventimiglia, "A facile and fast chemical process to manufacture epoxy–silane coating on plastic substrate for biomolecules sensing applications," *BioNanoSci.*, vol. 4, no. 3, pp. 226–231, 2014.

[13] C. B. Rosen, D. Rodriguez-Larrea, and H. Bayley, "Single-molecule site-specific detection of protein phosphorylation with a nanopore," *Nature Biotechnol.*, vol. 32, no. 2, pp. 179–181, 2014.

[14] A. Akbarzadeh, M. Samiei, and S. Davaran, "Magnetic nanoparticles: Preparation, physical properties, and applications in biomedicine," *Nanoscale Res. Lett.*, vol. 7, no. 1, pp. 1–13, 2012.

[15] X. Wang, Y. Chen, H. Xi, H. Li, and D. Dimitrov, "Spintronic memristor through spin-torque-induced magnetization motion," *IEEE Electron Device Lett.*, vol. 30, no. 3, pp. 294–297, Mar. 2009.

[16] Y. Chen, X. Wang, Z. Sun, and H. Li, "The application of spintronic devices in magnetic bio-sensing," in *Proc. 2nd Asia Symp. Quality Electron. Design*, 2010, pp. 230–234.

[17] L. Chua, "Memristor—The missing circuit element," *IEEE Trans. Circuit Theory*, vol. 18, no. 5, pp. 507–519, 2002.

[18] X. Wang, Y. Chen, Y. Gu, and H. Li, "Spintronic memristor temperature sensor," *IEEE Electron Device Lett.*, vol. 31, no. 1, pp. 20–22, Jan. 2010.

[19] X. Wang, Q. Shao, C. Leung, and A. Ruotolo, "Non-volatile, reversible switching of the magnetic moment in mn-doped zno films," *J. Appl. Phys.*, vol. 113, no. 17, p. 17C301, 2013.

[20] Z. Hu *et al.*, "Ferroelectric memristor based on pt/$BiFeO_3$/nb-doped $SrTiO_3$ heterostructure," *Appl. Phys. Lett.*, vol. 102, no. 10, p. 102901, 2013.

[21] A. Radoi, M. Dragoman, and D. Dragoman, "Memristor device based on carbon nanotubes decorated with gold nanoislands," *Appl. Phys. Lett.*, vol. 99, no. 9, p. 093102, 2011.

[22] S. Wang and G. Li, "Advances in giant magnetoresistance biosensors with magnetic nanoparticle tags: Review and outlook," *IEEE Trans. Magn.*, vol. 44, no. 7, pp. 1687–1702, Jul. 2008.

[23] W. Brown, "Thermal fluctuations of a single-domain particle," *Phys. Rev.*, vol. 130, no. 5, pp. 1677–1686, 1963.

[24] L. Berger, "Emission of spin waves by a magnetic multilayer traversed by a current," *Phys. Rev. B*, vol. 54, no. 13, pp. 9353–9358, 1996.

[25] R. Duine, A. Nunez, and A. MacDonald, "Thermally assisted current-driven domain-wall motion," *Phys. Rev. Lett.*, vol. 98, no. 5, p. 56605, 2007.

[26] Y. Cao, T. Sato, M. Orshansky, D. Sylvester, and C. Hu, "New paradigm of predictive MOSFET and interconnect modeling for early circuit simulation," in *Proc. IEEE Custom Integrated Circuits Conf.*, 2000, pp. 201–204.

[27] L. J. Cimini, Jr., "Analysis and simulation of a digital mobile channel using orthogonal frequency division multiplexing," *IEEE Trans. Commun.*, vol. 33, no. 7, pp. 665–675, Jul. 1985.

[28] W. A. Shay, “Time division multiplexing,” in *Handbook of Computer Networks: Key Concepts, Data Transmission, and Digital and Optical Networks*. New York: Wiley, vol. 1, pp. 568–578.

[29] C. Reig, M.-D. Cubells-Beltrán, and D. R. Muñoz, “Magnetic field sensors based on giant magnetoresistance (GMR) technology: Applications in electrical current sensing,” *Sensors*, vol. 9, no. 10, pp. 7919–7942, 2009.

[30] A. Vatankhahghadim, S. Huda, and A. Sheikholeslami, “A survey on circuit modeling of spin-transfer-torque magnetic tunnel junctions,” *IEEE Trans. Circuits Syst. I, Reg. Papers*, vol. 61, no. 9, pp. 2634–2643, Sep. 2014.

[31] H. H. Li and M. Hu, “Compact model of memristors and its application in computing systems,” in *Proc. Conf. Design, Automat. Test Eur.*, 2010, pp. 673–678.

[32] G. Li *et al.*, “Detection of single micron-sized magnetic bead and magnetic nanoparticles using spin valve sensors for biological applications,” *J. Appl. Phys.*, vol. 93, p. 7557, 2003.

[33] D. Niu, Y. Chen, C. Xu, and Y. Xie, “Impact of process variations on emerging memristor,” in *Proc. 47th ACM/IEEE Design Automat. Conf. (DAC)*, 2010, pp. 877–882.

[34] J. Rajendran, H. Maenm, R. Karri, and G. S. Rose, “An approach to tolerate process related variations in memristor-based applications,” in *Proc. 24th Int. Conf. VLSI Design*, 2011, pp. 18–23.

[35] P. Szendro, G. Vincze, and A. Szasz, “Pink-noise behaviour of biosystems,” *Eur. Biophys. J.*, vol. 30, no. 3, pp. 227–231, 2001.

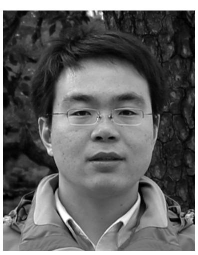

Jianlei Yang (S'12) received the B.S. degree in microelectronics from Xidian University, Xi'an, China, in 2009, and the Ph.D. degree in computer science and technology with Tsinghua University, Beijing, China, in 2014.

He is currently a post-doctoral researcher with the Department of Electrical and Computer Engineering, University of Pittsburgh, Pittsburgh, PA, USA. From 2013 to 2014, he was a research intern at Intel Labs China, Intel Corporation. His current research interests include numerical algorithms for VLSI power grid analysis and verification, spintronics and neuromorphic computing.

Dr. Yang was the recipient of the first place on TAU Power Grid Simulation Contest in 2011, and the second place on TAU Power Grid Transient Simulation Contest in 2012. He was a recipient of IEEE ICCD Best Paper Award in 2013, and ACM GLSVLSI Best Paper Nomination in 2015.

Zhenyu Sun (S'08) received the B.S. degree in microelectronics from East China Normal University, Shanghai, China, and the M.S. degree from the Department of Electrical and Computer Engineering, Polytechnic Institute of New York University, Brooklyn, NY, USA. He is currently pursuing the Ph.D. degree with the Department of Electrical and Computer Engineering, University of Pittsburgh, Pittsburgh, PA, USA.

His current research interests include architecture/circuit/device co-design and optimization for high performance, low power, and process variation tolerable eNVM system.

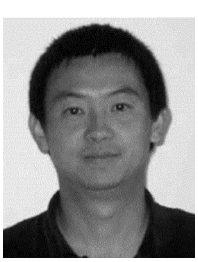

Xiaobin Wang (M'03) received the Ph.D. degree in physics from the University of California, San Diego (UCSD), CA, USA, in 2003. At UCSD, he was a graduate research assistant under Prof. H. N. Bertram, where his study was focused on dynamic thermal magnetization switching and magnetization noise in data storage devices.

He has been with Seagate Technology, Bloomington, MN, since 2003. His work at Seagate Technology includes advanced transducer modeling, design and testing, prediction of storage and memory system performance, alternative technology investigation, and intellectual property analysis. He published over 50 papers and had over 30 U.S. patents pending. He was invited to contribute at various conferences and journal reviews.

Yiran Chen (M'08) received the B.S. and M.S. (Hons.) degrees from Tsinghua University, Beijing, China, and the Ph.D. degree from Purdue University, West Lafayette, IN, USA.

He joined the University of Pittsburgh, Pittsburgh, PA, USA, in 2010, where he is currently an Assistant Professor with the Electrical and Computer Engineering Department. He has published one book, a few book chapters, and more than 130 technical publications in refereed journals and conferences. He has granted 73 U.S. patents with other 20 pending applications. His current research interests include low-power design, emerging technologies, and embedded system. He is an Associate Editor of the ACM *Journal of Emerging Technologies in Computing Systems*.

Dr. Chen is an Associate Editor of the IEEE TRANSACTIONS ON COMPUTER-AIDED DESIGN OF INTEGRATED CIRCUITS AND SYSTEMS. He has been involved in various roles in technical and organization committees of many international conferences, including DAC, ICCAD, DATE, ASP-DAC, ISLPED, FPT, ISCAS, CODES+ISSS, ICONIP, and RTCAS. He received The hot 100 products of 2006 from EDN, the finalist of Prestigious 2007 DesignVision Awards from the International Engineering Consortium and PrimeTimeVX–EDN 100 Hot Products Distinction from Synopsys Inc. He received three Best Paper Awards from ISQED in 2008, ISLPED in 2010, GLSVLSI in 2013, and other Best Paper Nominations from ISQED, DATE, and ASP-DAC. He received the 49th DAC A. Richard Newton Scholarship. He is a recipient of the National Science Foundation CAREER Award in 2013.

Hai Li (M'08) received the B.S. and M.S. degrees in microelectronics from Tsinghua University, Beijing, China, and the Ph.D. degree from the Electrical and Computer Engineering Department at Purdue University, West Lafayette, IN, USA, in 2004.

She is currently an Associate Professor with the Department of Electrical and Computer Engineering, University of Pittsburgh, Pittsburgh, PA, USA. At her early career, she worked with Qualcomm Inc., Intel Corp., Seagate Technology, and Polytechnic Institute of New York University. Her research interests include memory design and architecture, neuromorphic architecture for brain-inspired computing systems, and architecture/circuit/device cross-layer optimization for low power and high performance. She authored and co-authored over 100 technical papers published in peer-reviewed journals and conferences and holds 67 granted U.S. patents. Her book “Nonvolatile Memory Design: Magnetic, Resistive, and Phase Changing” was published by CRC Press in 2011. . She is the Associate Editor of the ACM *Transactions on Design Automation of Electronic Systems*.

Dr. Li received five best paper awards and five best paper nominations from ISQED, ISLPED, DATE, ISVLSI, ASPDAC, and ICCAD. She is the Associate Editor of the IEEE TRANSACTIONS ON VERY LARGE SCALE INTEGRATION (VLSI) SYSTEMS, IEEE TRANSACTIONS ON MULTI-SCALE COMPUTING SYSTEMS, and has served as technical program committee members for more than 20 international conference series. She is the recipient of NSF CAREER award in 2012 and DARPA YFA award in 2013.